

# Journal of Materials Chemistry A

Accepted Manuscript



This is an *Accepted Manuscript*, which has been through the Royal Society of Chemistry peer review process and has been accepted for publication.

*Accepted Manuscripts* are published online shortly after acceptance, before technical editing, formatting and proof reading. Using this free service, authors can make their results available to the community, in citable form, before we publish the edited article. We will replace this *Accepted Manuscript* with the edited and formatted *Advance Article* as soon as it is available.

You can find more information about *Accepted Manuscripts* in the [Information for Authors](#).

Please note that technical editing may introduce minor changes to the text and/or graphics, which may alter content. The journal's standard [Terms & Conditions](#) and the [Ethical guidelines](#) still apply. In no event shall the Royal Society of Chemistry be held responsible for any errors or omissions in this *Accepted Manuscript* or any consequences arising from the use of any information it contains.

## 3D Mesoporous Hybrid NiCo<sub>2</sub>O<sub>4</sub>@graphene Nanoarchitectures as Electrode Materials for Supercapacitors with Enhanced Performances

Cite this: DOI: 10.1039/x0xx00000x

Received 00th January 2012,  
Accepted 00th January 2012

DOI: 10.1039/x0xx00000x

www.rsc.org/

Yiying Wei<sup>a, b</sup>, Shuangqiang Chen<sup>a</sup>, Dawei Su<sup>a</sup>, Bing Sun<sup>a</sup>, Jianguo Zhu<sup>\*b</sup> and Guoxiu Wang<sup>\*a</sup>

3D mesoporous hybrid NiCo<sub>2</sub>O<sub>4</sub>@graphene nanoarchitectures were successfully synthesized by a combination of freeze drying and hydrothermal reaction. Field-emission scanning electron microscopy (FESEM) and TEM analyses revealed that NiCo<sub>2</sub>O<sub>4</sub>@graphene nanostructures consist of a hierarchical mesoporous sheet-on-sheet nanoarchitecture with a high specific surface area of 194 m<sup>2</sup> g<sup>-1</sup>. Ultrathin NiCo<sub>2</sub>O<sub>4</sub> nanosheets, with a thickness of a few nanometers and mesopores ranging from 2 to 5 nm, were wrapped in graphene nanosheets and formed hybrid nanoarchitectures. When applied as electrode materials in supercapacitors, hybrid NiCo<sub>2</sub>O<sub>4</sub>@graphene nanosheets exhibited a high capacitance of 778 F g<sup>-1</sup> at the current density of 1 A g<sup>-1</sup>, and an excellent cycling performance extending to 10000 cycles at the high current density of 10 A g<sup>-1</sup>.

### Introduction

Supercapacitor, also known as ultracapacitor, is a prevailing energy storage device, which has been intensively investigated. It possesses higher energy density than traditional electrolytic capacitors, and has much higher power density than rechargeable batteries. There are two types of supercapacitors, with each using different energy storage mechanisms: electrochemical double layer capacitors (EDLC) <sup>1-5</sup> and pseudocapacitors. <sup>6-10</sup> The EDLCs store energy in the electrostatic field, which is between electrode active materials and the electrolyte. Pseudocapacitors mainly rely on fast and reversible redox reactions. Transition metal oxides are usually employed as electrode materials for pseudocapacitors. However, pure transition metal oxides always suffer from low conductivity, resulting in unsatisfactory performances.

It is well recognised that combining conductive materials and transition metal oxides as composites is an effective method to improve the performance of supercapacitors. Graphene, a 2D monolayer of sp<sup>2</sup>-hybridized carbon atoms, possesses high conductivity, good mechanical strength, and ultra-large specific surface area, making it a suitable candidate as the conductive material. <sup>3, 11-16</sup> Many transition metal oxides <sup>17-24</sup> have been investigated as electrode materials for supercapacitors. NiCo<sub>2</sub>O<sub>4</sub> is one of the most promising transition metal oxides for pseudocapacitors owing to its intriguing electronic conductivity, low diffusion resistance to protons/cations, and easy electrolyte penetration. <sup>25-28</sup> In the crystal structure of NiCo<sub>2</sub>O<sub>4</sub>, nickel occupies the octahedral

sites and cobalt distributes over both octahedral and tetrahedral sites, in which the solid-state redox couples Co<sup>3+</sup>/Co<sup>2+</sup> and Ni<sup>3+</sup>/Ni<sup>2+</sup> are presented. <sup>25</sup>

Many studies focused on the optimization of morphology and incorporating NiCo<sub>2</sub>O<sub>4</sub> with conductive materials to obtain high specific capacitance. Wei *et al.* synthesized spinel nickel cobaltite aerogels with a high specific capacitance at the sweep rate of 25 mV s<sup>-1</sup>. <sup>27</sup> Yuan *et al.* demonstrated ultrathin mesoporous NiCo<sub>2</sub>O<sub>4</sub> nanosheets growing on Ni foam by co-electro-deposition of Ni and Co. <sup>28</sup> Furthermore, Zhang *et al.* prepared mesoporous NiCo<sub>2</sub>O<sub>4</sub> nanosheets on Ni foam, Ti foil, stainless-steel foil and flexible graphite paper, <sup>29, 30</sup> and nanoneedle arrays on carbon nanofiber, <sup>26</sup> exhibiting high capacitance and cycling stability. However, most of these are plagued by poor high-rate performances.

Herein, we report the synthesis of mesoporous and macroporous hybrid NiCo<sub>2</sub>O<sub>4</sub>/graphene nanostructures, in which ultrathin NiCo<sub>2</sub>O<sub>4</sub> nanosheets are interconnected with each other, forming 3D nanoarchitectures with a high surface area of 194 m<sup>2</sup> g<sup>-1</sup>. When applied as electrode materials in supercapacitors, these novel 3D hierarchical porous nanoarchitectures exhibited high specific capacitances and excellent cycling stabilities at high current densities.

### Experimental

#### Fabrication of graphene – polyurethane (PU) sponges

Graphene oxide (GO) was prepared from natural graphite flakes by a modified Hummers method, <sup>31</sup> and the GO nanosheets were

## Paper

dispersed in 20 mL DI water at the concentration of  $2 \text{ mg mL}^{-1}$  by stirring for 12 hours and ultrasonicated (Branson 2510) for 2 hours at room temperature. After dispersion, the homogeneous solution in the vial was transferred to a beaker for stable dispersion. This involved adding 80 mg sodium cholate hydrate (SCH) to the mixture and stirring for 2 hours. Hydrazine solution (35 wt% in water, Aldrich) at the weight ratio of 1:7 was subsequently added to the beaker to obtain the reduced graphene oxide (RGO) solution.<sup>32</sup> The polyurethane (PU)-sponge was cleaned several times using distilled water and acetone, completely dried in a vacuum, and then cut into small pieces, with a thickness of 1 mm and a width by length of  $2 \times 2 \text{ cm}^2$ . In a glass tube, three PU-sponge pieces were immersed in 20 ml of the mixture solution, under microwave irradiation at  $90^\circ \text{C}$  for 30 mins (pressure:  $\sim 8 \text{ Bar}$ ) in a single mode microwave reactor (Nova, EU Microwave Chemistry). After freeze-drying for 48 hours, the solvent within the material was completely removed, and the RGO-PU-sponges were obtained.

### Preparation of $\text{NiCo}_2\text{O}_4$ @graphene nanoarchitectures

1 mmol of  $\text{Ni}(\text{NO}_3)_2 \cdot 6\text{H}_2\text{O}$ , 2 mmol of  $\text{Co}(\text{NO}_3)_2 \cdot 6\text{H}_2\text{O}$  and 4.5 mmol of hexamethylenetetramine were dissolved in 40 mL of DI water to form a transparent pink solution. 10 ml solution was transferred to a Teflon-lined Autoclave, with one piece of graphene-PU-sponge, and then heated under a hydrothermal condition of  $90^\circ \text{C}$  for 12 hours. The as-prepared black materials were washed several times with distilled water and ethanol, and dried under vacuum condition of  $80^\circ \text{C}$  for 12 hours. This was followed by annealing at  $350^\circ \text{C}$  for 2 hours with a slow heating rate of  $1^\circ \text{C min}^{-1}$ , in order to achieve 3D mesoporous  $\text{NiCo}_2\text{O}_4$  on large-size graphene hybrid nanostructures. Using the same procedure, the bare  $\text{NiCo}_2\text{O}_4$  without graphene was also prepared.

### Materials characterization

The crystal structure and phase of the as-prepared materials

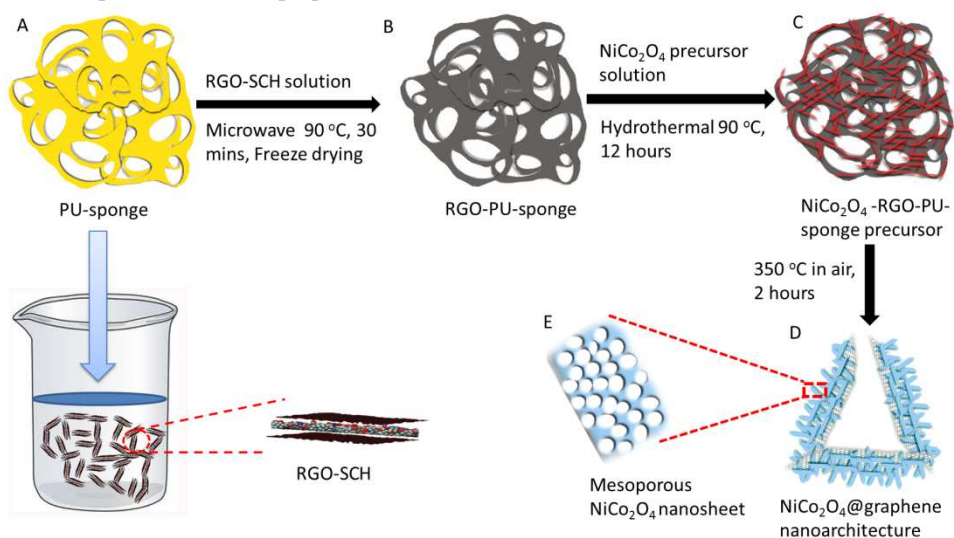


**Fig. 1** Synthesis process of  $\text{NiCo}_2\text{O}_4$ @graphene nanoarchitectures: (A) a piece of PU-sponge and the solution with RGO stabilized using sodium cholate hydrate (SCH); (B) The RGO was coated and anchored onto the PU-sponge assisted by microwave and freeze drying; (C)  $\text{NiCo}_2\text{O}_4$  precursor nanosheets grown on RGO-PU-sponges; (D) 3D mesoporous hybrid  $\text{NiCo}_2\text{O}_4$ @graphene nanoarchitectures. (E) Crystallized  $\text{NiCo}_2\text{O}_4$  nanosheets with mesopores.

## Journal of Materials Chemistry A

were characterized by X-ray diffraction (XRD) (Siemens D5000 X-ray diffractionmeter) using  $\text{Cu K}\alpha$  radiation with  $2\theta$  ranging from  $10^\circ$  to  $80^\circ$ . The morphology and crystal structures were characterized by field-emission scanning electron microscopy (FE-SEM, JSM-6700F), and transmission electron microscopy/selected area electron diffraction (TEM/SAED, JEOL JEM-200CX) equipped with an energy-dispersive X-ray spectrometer (EDX).  $\text{N}_2$  adsorption-desorption measurements were conducted using a 3 Flex surface characterization analyser at 77 K.

### Electrochemical testing

To prepare the working electrode, the as-prepared materials (80 wt %), acetylene black (15 wt %), and poly(vinylidene fluoride) (PVDF, 5 wt %) were mixed in N-methyl-2-pyrrolidone (NMP) to form a slurry. The resultant slurry was pasted onto Ni foam (washed by 10 wt% HCl) with a blade, and then dried at  $80^\circ \text{C}$  for 12 hours under vacuum. The nickel foam was initially cleaned before using as the current collector. It was immersed into acetone for 10 minutes followed by ultra-sonication for 5 minutes. The nickel foam was then cleaned by 0.1 M hydrochloric acid. After then, it was washed by distilled water with ultra-sonication for 5 minutes. Electrochemical measurements were carried out using three-electrode cells, with platinum as the counter electrode and a saturated calomel electrode (SCE) as the reference electrode. Cyclic voltammetry (CV) and galvanostatic charge-discharge (CD) was carried out on a CHI 660C electrochemistry workstation using 2.0 M KOH electrolyte. Electrochemical impedance spectroscopy (EIS) measurements were conducted by applying an AC voltage with 1 mV amplitude in a frequency range of 0.01 Hz to 100 kHz at the open circuit potential.

### Results and Discussion

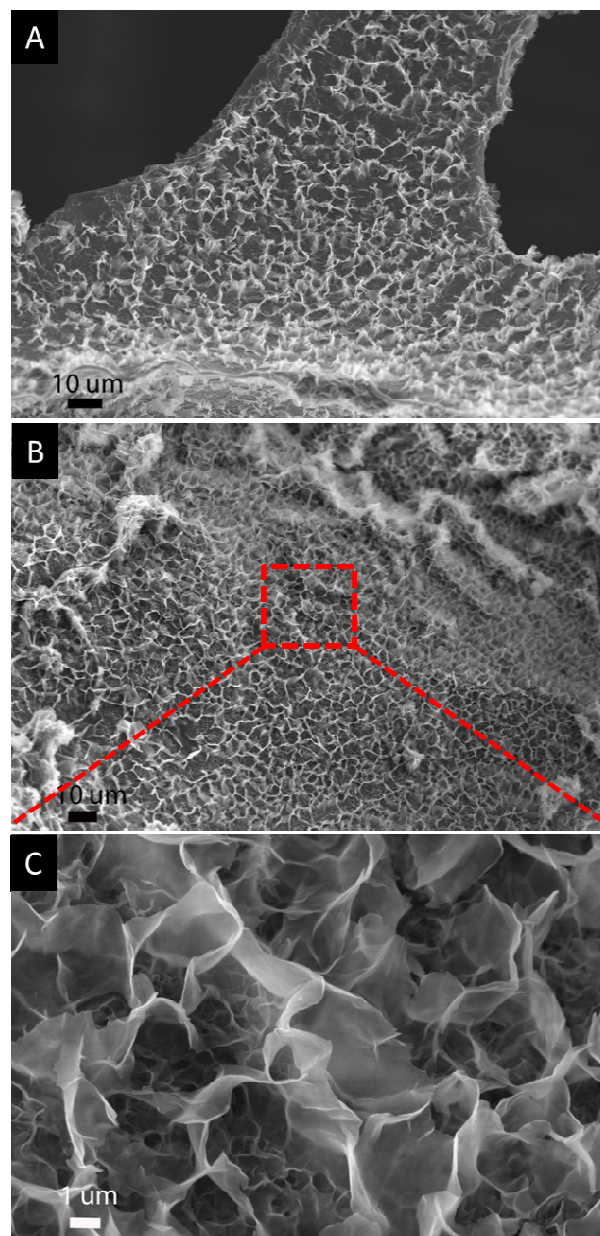


**Fig. 2** SEM images of (A, B)  $\text{NiCo}_2\text{O}_4$  precursor sheets that grew on the skeleton of RGO-PU-sponge; (C) high magnification SEM image of  $\text{NiCo}_2\text{O}_4$  precursor with macropores.

Fig. 1 illustrates the preparation process for the synthesis of hybrid  $\text{NiCo}_2\text{O}_4$ @graphene nanoarchitectures. In the first step, the commercial PU-sponge was cut into ribbons (Fig. 1A). The planar amphiphilic surfactant SCH enables the formation of a stable encapsulation layer on each side of the suspended graphene sheets, leading to stable dispersion of graphene in deionized water.<sup>17, 33-35</sup> Owing to the planar nanosheet structure of graphene and the strong van der Waals force between the PU-sponge and RGO-SCH, the dispersed graphene can be easily and uniformly coated onto the surface of the PU-sponge's skeleton by using a microwave-assisted method and a further treatment of freeze drying (Fig. 1B). The next step was

to grow a  $\text{NiCo}_2\text{O}_4$  precursor onto the RGO-PU-sponge skeleton by the hydrothermal method as shown in Fig. 1C. Hexamethylenetetramine, nickel (II) nitrate hexahydrate crystalline and cobalt (II) nitrate hexahydrate were used to hydrothermally grow  $\text{NiCo}_2\text{O}_4$  nanosheet precursors on RGO-PU-sponges. The  $\text{NiCo}_2\text{O}_4$  nanosheet precursors consist of bimetallic (Ni, Co) hydroxide. Upon the annealing treatment (Fig. 1D), crystallized  $\text{NiCo}_2\text{O}_4$  nanosheets with mesopores (Fig. 1E) on large-size graphene sheets were obtained.

The SEM observation identified that the PU-sponge has pore size ranging from 50  $\mu\text{m}$  to 500  $\mu\text{m}$  (Fig. S1A and S1B in

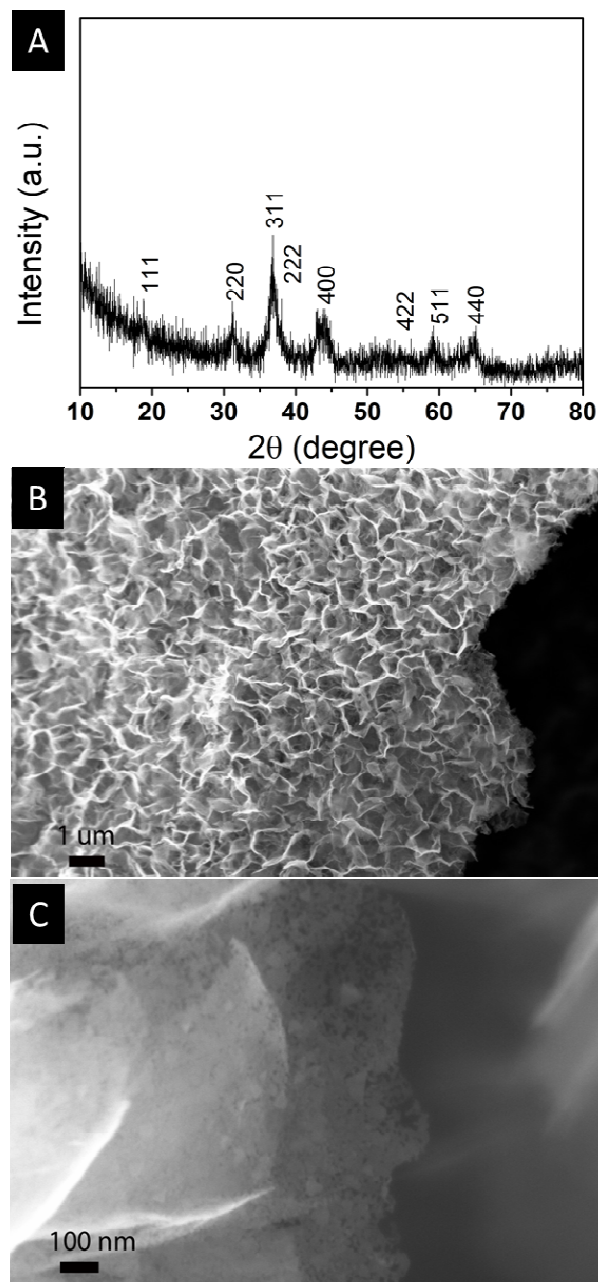


**Fig. 3** (A) XRD pattern of  $\text{NiCo}_2\text{O}_4$ @graphene nanoarchitectures. (B) SEM image of foam-like hybrid  $\text{NiCo}_2\text{O}_4$ @graphene nanoarchitectures with hierarchical pores. (C) SEM image of  $\text{NiCo}_2\text{O}_4$  nanosheets.

## Paper

## Journal of Materials Chemistry A

Electronic Supplementary Information (ESI)). After coating with graphene, the PU-sponges preserved the hierarchical macroporous structure. It allows for the flow of the precursor solution into the pores of RGO-PU-sponge, and  $\text{NiCo}_2\text{O}_4$  nanosheet precursors to grow on the surface of the skeleton. The surface of PU-sponges changed from smooth to corrugated after being coated with the RGO (Fig. S1C and S1D in ESI). The SEM observation clearly confirmed that graphene nanosheets have been successfully coated onto the surface of PU-sponges.

SEM images of  $\text{NiCo}_2\text{O}_4$ -RGO-PU-sponge precursors clearly show a 3D hierarchical porous structure. Fig. 2A and 2B illustrate that  $\text{NiCo}_2\text{O}_4$  precursor nanosheets grew on the conductive RGO-PU-sponges. In the inner region (Fig. 2C), the  $\text{NiCo}_2\text{O}_4$  precursor nanosheets are interconnected with each other to form the macroporous structure. It should be noted that  $\text{NiCo}_2\text{O}_4$  precursor nanosheets grew vertically to the graphene nanosheet substrates.

After having been annealed at 350 °C in air for 2 hours, the final product materials were characterized by XRD, SEM and TEM. Fig. 3A shows the XRD pattern of the 3D mesoporous  $\text{NiCo}_2\text{O}_4$ @graphene nanoarchitectures. Seven diffraction peaks were observed at the  $2\theta$  of 18.9°, 31.1°, 36.6°, 44.6°, 59.1°, 64.9° and 68.3°. All the peaks can be indexed to the standard spinel  $\text{NiCo}_2\text{O}_4$  crystalline structure, with the indices of (111), (220), (311), (400), (422), (511) and (440) (JCPDF-20-0781). After annealing, the morphologies of the 3D porous structure were well preserved. PU-sponges were completely burnt out at 350 °C in air. The  $\text{NiCo}_2\text{O}_4$ @graphene nanosheets retained the 3D shape of the PU-sponge (Fig. S2A in ESI). A foam-like nanoarchitecture consisting of hierarchical pores was obtained (as shown in Fig. 2SA and 2SB, ESI). From the magnified view (Fig. 3B), porous  $\text{NiCo}_2\text{O}_4$  nanosheets can be observed. Furthermore, the highly magnified SEM image of the crystalline  $\text{NiCo}_2\text{O}_4$  nanosheets (Fig. 3C) clearly shows the presence of the mesoporous structure of the ultra-thin  $\text{NiCo}_2\text{O}_4$  nanosheets.

TEM images also revealed that  $\text{NiCo}_2\text{O}_4$ @graphene nanosheets contain porous 3D architectures with mesopores and macropores. The macropores (50 – 200 nm) are formed by the interconnection of  $\text{NiCo}_2\text{O}_4$  nanosheets, which are clearly visible in Fig. 4A and Fig. S2C in ESI. The mesopores, ranging from 2 to 5 nm, are uniformly distributed on the  $\text{NiCo}_2\text{O}_4$  nanosheets, which grew on large-size graphene sheets (as shown in Fig. 4B and Fig. S2D in ESI). As shown in the inset image of Fig. 4B, the corresponding crystalline diffraction rings of (311), (400), (440) and (620) in the selected area electron diffraction (SAED) pattern confirmed the polycrystalline  $\text{NiCo}_2\text{O}_4$ . Furthermore, HRTEM image (Fig. 4C) demonstrates that the  $\text{NiCo}_2\text{O}_4$  nanosheets are well-crystallized with an interplanar (022) space of 0.23 nm.

The pore-size features of the 3D mesoporous hybrid  $\text{NiCo}_2\text{O}_4$ @graphene nanoarchitectures were further measured by nitrogen adsorption/desorption isotherms. The Brunauer–Emmett–Teller (BET) surface area is determined by the nitrogen adsorption/desorption at 77 K. The isotherm of the

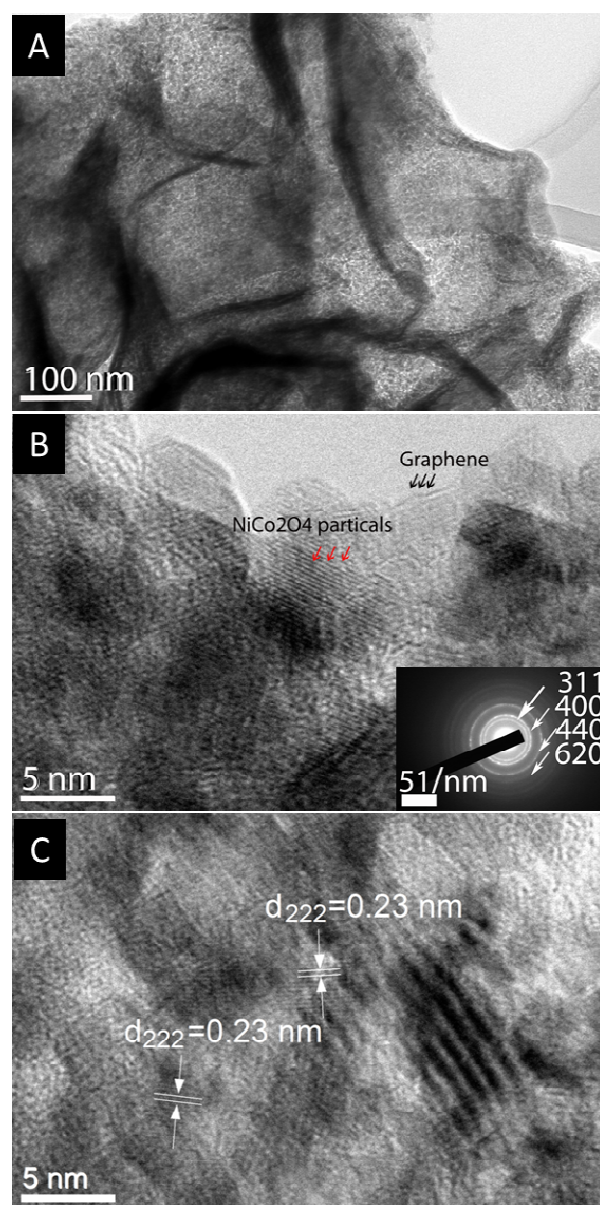


**Fig. 4** (A) TEM image of  $\text{NiCo}_2\text{O}_4$ @graphene nanosheets, showing the porous architecture. (B) HRTEM images of  $\text{NiCo}_2\text{O}_4$ @graphene nanosheets. The inset SAED pattern can be fully indexed to polycrystalline  $\text{NiCo}_2\text{O}_4$ . (C) Lattice resolved HRTEM image of  $\text{NiCo}_2\text{O}_4$  nanosheets.

material exhibits the characteristics of type II and VI isotherms, which indicates the combination of macropores and mesopores<sup>36</sup> (Fig. S3A in ESI). Because of the 3D hierarchical porous structure, a large surface area of 195.4  $\text{m}^2 \text{g}^{-1}$  and the total pore volume ratio of 0.27  $\text{cm}^3 \text{g}^{-1}$  were achieved. The corresponding pore size distribution (Fig. S3B in ESI) indicates a pore size range of 2–5 nm, which is consistent with the SEM and TEM observations.

The electrochemical performances of the 3D porous hybrid  $\text{NiCo}_2\text{O}_4$ @graphene nanoarchitectures were tested as the electrodes for supercapacitors. As shown in Fig. 5A and B, the electrodes are able to function in a wide range of scan rates, ranging from 5  $\text{mV s}^{-1}$  up to 200  $\text{mV s}^{-1}$ . The shape of the CV

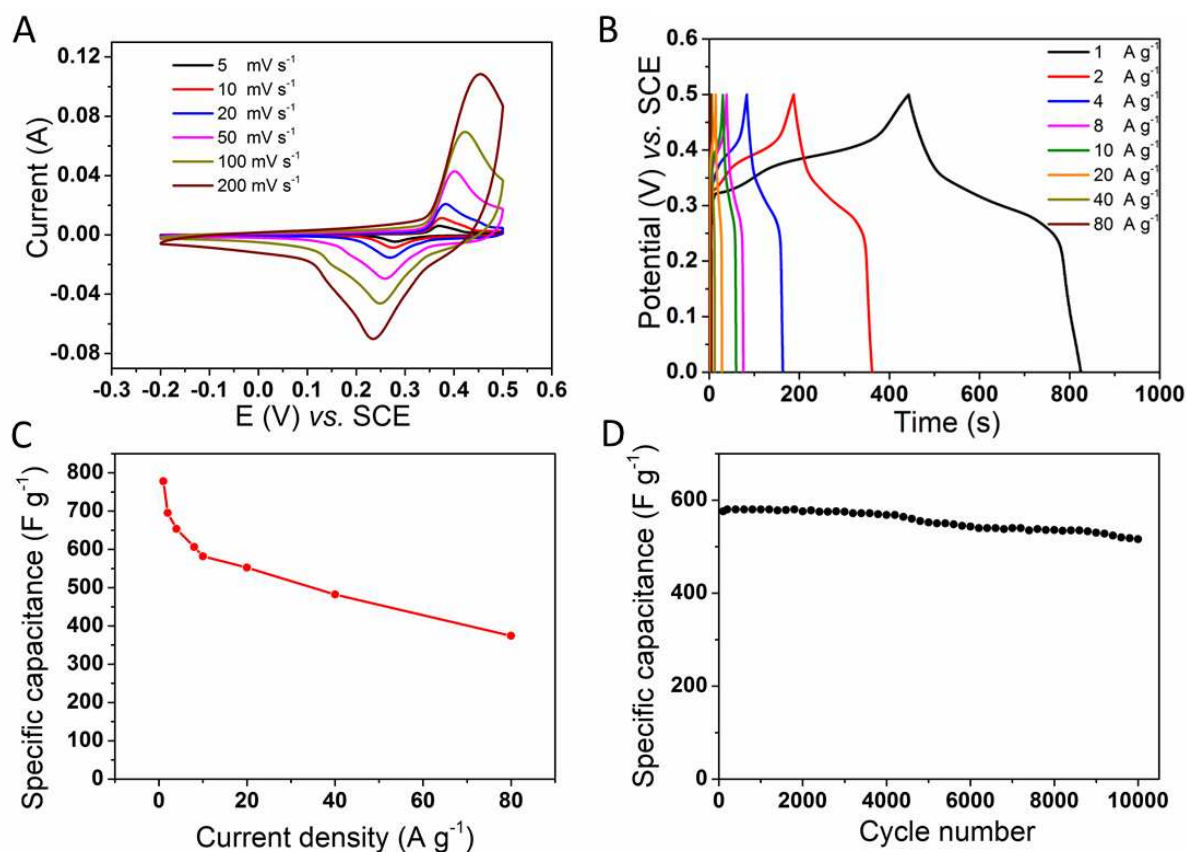


**Fig. 5** Electrochemical performance of the NiCo<sub>2</sub>O<sub>4</sub>@graphene nanoarchitectures. (A) CV curves at the scan rate of 5 mV s<sup>-1</sup> to 200 mV s<sup>-1</sup>; (B) constant-current charge/discharge profile at the current densities of 1 A g<sup>-1</sup> to 80 A g<sup>-1</sup>; (C) specific capacitance vs current density; (D) capacity retention vs cycle number up to 10,000 cycles at 10 A g<sup>-1</sup>. All the data are taken in 2.0 M KOH electrolyte.

curves clearly reveals the characteristic of pseudocapacitors with a pair of redox peaks existing in the potential range of -0.2 to 0.5 V vs. SCE at all scan rates, even at a high scan rate of 200 mV s<sup>-1</sup>. The oxidation peak locates at 0.37 V and the reduction peak is at 0.28 V. The NiCo<sub>2</sub>O<sub>4</sub>@graphene electrodes are tolerant to a high scan rate, which indicates good conductivity and good charge propagation within the electrodes.<sup>37</sup> For the carbon-based electrode, the shape of the CV curve degrades significantly with the increase of the scan rate. On the contrary, the 3D NiCo<sub>2</sub>O<sub>4</sub>@graphene electrodes maintain the shape of the pseudocapacitance curve, even at high scan rates. The 3D porous nanoarchitectures, highly conductive graphene and high reactivity of NiCo<sub>2</sub>O<sub>4</sub> jointly contribute to such a high rate performance. With the increase of the scan rate, there is a little shift of the redox peaks, suggesting low polarization.<sup>28</sup> To further investigate the electrochemical characteristics of the as-prepared materials, galvanostatic charge-discharge measurements were carried out in 2M KOH electrolyte at various current densities. As shown in Fig. 5B, the supercapacitor operates well within a wide range of current densities, from 1 A g<sup>-1</sup> to 80 A g<sup>-1</sup>. This clearly demonstrates the excellent electrochemical performances of the 3D porous hybrid NiCo<sub>2</sub>O<sub>4</sub>@graphene nanoarchitectures.

Based on the charging/discharging curves, and the equation:

$$C = (I \times \Delta t) / (m \times \Delta v)$$

where  $I$  is the discharge current,  $\Delta t$  is the discharge time,  $\Delta v$  is the voltage range and  $m$  is the mass of the active material, the calculated specific capacitance as the function of discharging current density was plotted in Fig. 5C. The nickel foam will contribute to the capacitance in KOH electrolyte when it was used as the current collector.<sup>38</sup> The specific capacitance of bare nickel foam was measured (Fig. S5) and subtracted from the capacitance value of the material. NiCo<sub>2</sub>O<sub>4</sub>@graphene electrodes show excellent specific capacitance of 778, 696, 653, 606, 582, 552, 482 and 374 F g<sup>-1</sup>, at current densities of 1, 2, 4, 8, 10, 20, 40 and 80 A g<sup>-1</sup>, respectively. The electrode still maintains a high specific capacitance of 374 F g<sup>-1</sup> at the high current density of 80 A g<sup>-1</sup>. This outstanding pseudocapacitor performance could be ascribed to good conductivity and the 3D porous structure of the materials. Large-size graphene nanosheets were formed by using freeze drying, which provided the high electrical conductive medium for the electron transport. The ultrathin NiCo<sub>2</sub>O<sub>4</sub> sheets lead to the high specific area to react with ions in the electrolyte. The uniform mesoporous and macroporous structure optimizes the ion diffusion path, and facilitates the adsorption/desorption of K<sup>+</sup> and the transportation of ions. This allows for the complete distribution of electrolyte into the electrode, and for

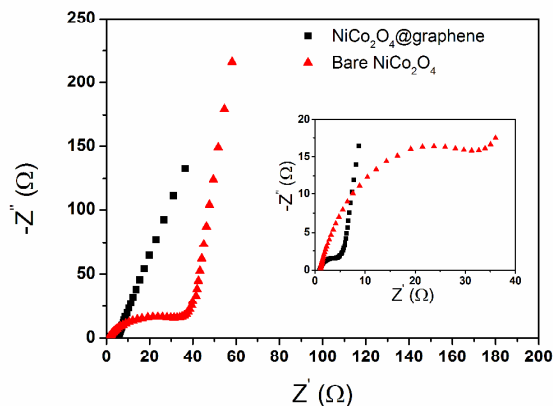


**Fig. 6** Nyquist plots of the a.c. impedance spectra of the porous NiCo<sub>2</sub>O<sub>4</sub>@graphene electrode and the bare NiCo<sub>2</sub>O<sub>4</sub> electrode in the frequency range from of 100 kHz to 0.01 Hz.

maximizing the utilization of the NiCo<sub>2</sub>O<sub>4</sub>. It ensures that there are efficient reactive sites between the NiCo<sub>2</sub>O<sub>4</sub> electrode and the electrolyte. In order to investigate the long-time cyclability, charge-discharge cycling up to 10,000 cycles has been conducted at the current density of 10 A g<sup>-1</sup> (as shown in Fig. 5D). Approximately 90% of the initial capacitance is retained after 10,000 cycles, demonstrating good cycling stability at high charge/discharge current density.

In order to further illustrate the advantages of porous NiCo<sub>2</sub>O<sub>4</sub>@graphene nanoarchitectures as electrode materials for supercapacitors, the electrochemical performances of the bare NiCo<sub>2</sub>O<sub>4</sub> were also evaluated. As shown in Fig. S4 (ESI), the bare NiCo<sub>2</sub>O<sub>4</sub> electrodes exhibited many poor performances at different current densities, compared with porous NiCo<sub>2</sub>O<sub>4</sub>@graphene electrodes. Fig. 6 shows the Nyquist plots of the a.c. impedance spectra of both the porous NiCo<sub>2</sub>O<sub>4</sub>@graphene electrode and the bare NiCo<sub>2</sub>O<sub>4</sub> electrode. It can be seen that the charge transfer resistance of the porous NiCo<sub>2</sub>O<sub>4</sub>@graphene electrode is much lower than that of the bare NiCo<sub>2</sub>O<sub>4</sub> electrode. Therefore, the unique porous NiCo<sub>2</sub>O<sub>4</sub>@graphene nanosheet architectures can significantly reduce the internal resistance (including solution resistance, charge transfer resistance and other resistances).<sup>6</sup> As shown in Table S1, compared to previous reports, the as-prepared materials achieved good cycleability at high current densities.

## Conclusions

In summary, we have successfully developed a novel synthetic method to prepare 3D porous NiCo<sub>2</sub>O<sub>4</sub>@graphene nanoarchitectures. The synthesis process involves coating of hydrazine-reduced graphene oxide onto the PU-sponge, and growing bimetallic (Ni, Co) ultrathin nanosheets. The final products consist of ultrathin NiCo<sub>2</sub>O<sub>4</sub> sheets with mesopores ranging from 2 to 5 nm. The mesoporous ultrathin NiCo<sub>2</sub>O<sub>4</sub> nanosheets also form the 3D macropores with the size in the range of 50 to 100nm. Owing to the 3D hierarchical porous structure, the NiCo<sub>2</sub>O<sub>4</sub>@graphene nanoarchitectures exhibit

high specific capacitance, an ultrafast charge/discharge rate, and excellent cycling stability. In particular, NiCo<sub>2</sub>O<sub>4</sub>@graphene nanoarchitectures delivered a high specific capacitance of 778 F g<sup>-1</sup> and 374 F g<sup>-1</sup> at the current densities of 1 A g<sup>-1</sup> and 80 A g<sup>-1</sup>, respectively.

## Acknowledgements

This research is financially supported by the Australia Research Council through the ARC Discovery Project (DP1093855) and partially supported by the Chinese Scholarship Council (CSC No. 2011912003).

## Notes and references

<sup>a</sup> Centre for Clean Energy Technology, University of Technology Sydney, 15 Broadway, Ultimo NSW 2007, Australia. E-mail: Guoxiu.Wang@uts.edu.au  
<sup>b</sup> Centre for Electrical Machines and Power Electronics, University of Technology Sydney, 15 Broadway, Ultimo, NSW 2007, Australia. E-mail: Jianguo.Zhu@uts.edu.au

† Electronic Supplementary Information (ESI) available: Experimental details, SEM image of pure PU-sponge, the PU-sponge coated with graphene oxide, SEM images and XRD pattern of Graphene-NiCo<sub>2</sub>O<sub>4</sub> hybrid structure after annealing, N<sub>2</sub> adsorption-desorption isotherm measurement results. See DOI: 10.1039/b000000x/

1. Y. Zhai, Y. Dou, D. Zhao, P. F. Fulvio, R. T. Mayes and S. Dai, *Advanced Materials*, 2011, **23**, 4828-4850.
2. X. Huang, Z. Zeng, Z. Fan, J. Liu and H. Zhang, *Advanced Materials*, 2012, **24**, 5979-6004.
3. Q. Cheng, J. Tang, J. Ma, H. Zhang, N. Shinya and L.-C. Qin, *Physical Chemistry Chemical Physics*, 2011, **13**, 17615-17624.
4. C. X. Guo and C. M. Li, *Energy & Environmental Science*, 2011, **4**.
5. C. Liu, Z. Yu, D. Neff, A. Zhamu and B. Z. Jang, *Nano Letters*, 2010, **10**, 4863-4868.
6. W. Chen, R. Rakhi, L. Hu, X. Xie, Y. Cui and H. Alshareef, *Nano letters*, 2011, **11**, 5165-5172.
7. L. Yan, S. Wu and W. Chen, *Journal of Materials Chemistry A*, 2013.
8. N. Mahmood, C. Zhang, H. Yin and Y. Hou, *Journal of Materials Chemistry A*, 2014.
9. M. Zhi, C. Xiang, J. Li, M. Li and N. Wu, *Nanoscale*, 2013, **5**, 72-88.
10. Z. Su, C. Yang, C. Xu, H. Wu, Z. Zhang, T. Liu, C. Zhang, Q. Yang, B. Li and F. Kang, *Journal of Materials Chemistry A*, 2013, **1**, 12432-12440.
11. J. J. Yoo, K. Balakrishnan, J. Huang, V. Meunier, B. G. Sumpter, A. Srivastava, M. Conway, A. L. Mohana Reddy, J. Yu, R. Vajtai and P. M. Ajayan, *Nano Letters*, 2011, **11**, 1423-1427.
12. Y. B. Tan and J.-M. Lee, *Journal of Materials Chemistry A*, 2013, **1**, 14814-14843.
13. M. Sawangphruk, M. Suksomboon, K. Kongsupornsak, J. Khuntilo, P. Srimuk, Y. Sanguansak, P. Klunbud, P. Suktha and P. Chiochan, *Journal of Materials Chemistry A*, 2013, **1**, 9630-9636.
14. S. Chen, W. Xing, J. Duan, X. Hu and S. Z. Qiao, *Journal of Materials Chemistry A*, 2013, **1**, 2941-2954.
15. M.-T. Lee, C.-Y. Fan, Y.-C. Wang, H.-Y. Li, J.-K. Chang and C.-M. Tseng, *Journal of Materials Chemistry A*, 2013, **1**, 3395-3405.

16. S. Wang and R. A. W. Dryfe, *Journal of Materials Chemistry A*, 2013, **1**, 5279-5283.
17. G. Yu, L. Hu, M. Vosgueritchian, H. Wang, X. Xie, J. R. McDonough, X. Cui, Y. Cui and Z. Bao, *Nano letters*, 2011, **11**, 2905-2911.
18. L. Peng, X. Peng, B. Liu, C. Wu, Y. Xie and G. Yu, *Nano letters*, 2013.
19. S. D. Perera, B. Patel, N. Nijem, K. Roodenko, O. Seitz, J. P. Ferraris, Y. J. Chabal and K. J. Balkus, *Advanced Energy Materials*, 2011, **1**, 936-945.
20. H. Zhao, L. Pan, S. Xing, J. Luo and J. Xu, *Journal of Power Sources*, 2013, **222**, 21-31.
21. C.-C. Hu, K.-H. Chang, M.-C. Lin and Y.-T. Wu, *Nano letters*, 2006, **6**, 2690-2695.
22. C.-C. Hu, W.-C. Chen and K.-H. Chang, *Journal of The Electrochemical Society*, 2004, **151**, A281-A290.
23. R.-R. Bi, X.-L. Wu, F.-F. Cao, L.-Y. Jiang, Y.-G. Guo and L.-J. Wan, *The Journal of Physical Chemistry C*, 2010, **114**, 2448-2451.
24. H. Wang, H. Yi, X. Chen and X. Wang, *Journal of Materials Chemistry A*, 2014.
25. B. Cui, H. Lin, J. B. Li, X. Li, J. Yang and J. Tao, *Advanced Functional Materials*, 2008, **18**, 1440-1447.
26. G. Q. Zhang, H. B. Wu, H. E. Hoster, M. B. Chan-Park and X. W. D. Lou, *Energy & Environmental Science*, 2012, **5**, 9453-9456.
27. T. Y. Wei, C. H. Chen, H. C. Chien, S. Y. Lu and C. C. Hu, *Advanced materials*, 2010, **22**, 347-351.
28. C. Yuan, J. Li, L. Hou, X. Zhang, L. Shen and X. W. D. Lou, *Advanced Functional Materials*, 2012, **22**, 4592-4597.
29. G. Zhang and X. W. D. Lou, *Advanced Materials*, 2012.
30. G. Zhang and X. W. D. Lou, *Scientific reports*, 2013, **3**.
31. W. S. Hummers Jr and R. E. Offeman, *Journal of the American Chemical Society*, 1958, **80**, 1339-1339.
32. B. G. Choi, M. Yang, W. H. Hong, J. W. Choi and Y. S. Huh, *ACS nano*, 2012, **6**, 4020-4028.
33. S. Mukhopadhyay and U. Maitra, *Current Science*, 2004, **87**, 1666-1683.
34. A. A. Green and M. C. Hersam, *Nano letters*, 2009, **9**, 4031-4036.
35. S. Lin, C.-J. Shih, M. S. Strano and D. Blankschtein, *Journal of the American Chemical Society*, 2011, **133**, 12810-12823.
36. Z. Ryu, J. Zheng, M. Wang and B. Zhang, *Carbon*, 1999, **37**, 1257-1264.
37. M. D. Stoller, S. Park, Y. Zhu, J. An and R. S. Ruoff, *Nano Letters*, 2008, **8**, 3498-3502.
38. W. Xing, S. Qiao, X. Wu, X. Gao, J. Zhou, S. Zhuo, S. B. Hartono and D. Hulicova-Jurcakova, *Journal of Power Sources*, 2011, **196**, 4123-4127.